A Second Order Finite Volume Technique for Simulating Transport in Anisotropic Media

Jayantha Pasdunkorale A. * Ian W. Turner †

Received in Septermber 2001, Accepted in August 2002

*Centre in Statistical Science and Industrial Mathematics, School of Mathematical Sciences, Gardens Point Campus, Queensland University of Technology, GPO Box 2434, Brisbane 4001, Australia, (On study leave from the Department of Mathematics, University of Ruhuna, Matara, Sri Lanka). email:pa.jayantha@fsc.qut.edu.au,jayanthapa@yahoo.com

†Centre in Statistical Science and Industrial Mathematics, School of Mathematical Sciences, Gardens Point Campus, Queensland University of Technology, GPO Box 2434, Brisbane 4001, Australia. email:i.turner@fsc.qut.edu.au

Keywords Flux Decomposition, Weighted Least Squares, Control Volume Technique, Orthotropic Media

Abstract

An existing two-dimensional finite volume technique is modified by introducing a correction term to increase the accuracy of the method to second order. It is well known that the accuracy of the finite volume method strongly depends on the order of the approximation of the flux term at the control volume (CV) faces. For highly orthotropic and anisotropic media, first order approximations produce inaccurate simulation results, which motivates the need for better estimates of the flux expression. In this article, a new approach to approximate the flux term at the CV face is presented. The discretisation involves a decomposition of the flux and an improved least squares approximation technique to calculate the derivatives of the dependent function on the CV faces for estimating both the cross diffusion term and a correction for the primary flux term. The advantage of this method is that any arbitrary unstructured mesh can be used to implement the technique without considering the shapes of the mesh elements. It was found that the numerical results well matched the available exact solution for a representative transport equation in highly orthotropic media and the benchmark solutions obtained on a fine mesh for anisotropic media. Previously proposed CV techniques are compared with the new method to highlight its accuracy for different unstructured meshes.

Nomenclature

A_k = Length of a control volume face $[m]$

C_p = Specific heat $[J/kg/K]$

F_k = midpoint of a control volume face

h_b = Heat transfer coefficient $[W/m^2/K]$

K = Conductivity tensor $[W/m/K]$

L = Dimension of the domain in the x direction $[m]$

M = Dimension of the domain in the y direction $[m]$

m = Order of the Taylor expansion

N = A representative node around a control volume

N_p = Number of nodes around a control volume

$\hat{\mathbf{n}}$ = Unit outward normal vector at a control volume face

P = Node surrounded by a control volume

R = Remainder of the Taylor expansion

S_b = Set of boundary points of the solution domain

t = Time $[s]$

$\hat{\mathbf{t}}$ = Unit vector perpendicular to $\mathbf{v}$

$\hat{\mathbf{u}}$ = Unit vector along a control volume face

$\mathbf{v}$ = Vector through a CV face connecting adjacent nodes $[m]$

$\mathbf{w}$ = the vector representing $K^T\hat{\mathbf{n}}$

x = Coordinate length $[m]$

y = Coordinate length $[m]$

Greek symbols

δt = Discrete time step size $[s]$

δV_P = Area of the control volume $[m^2]$

$\delta\underline{\mathrm{x}}$ = Vectors emanating from the midpoint of the face $[m]$

ϵ = Correction term in the approximation of primary flux term $[K]$

λ = A parameter in equation (10)

ρ = Density $[kg/m^3]$

ϕ = Transported quantity - Temperature $[K]$

ϕ_0 = Initial temperature $[K]$

ϕ_s = Surrounding temperature $[K]$

Superscripts and Subscripts

b = Boundary point

k = Index for the control volume faces

n = Represents n^{th} time step

Introduction

The finite volume technique is used extensively for solving a range of different problems arising in many fields of science, technology and engineering (Bailey *et al.* (1999), Davidson and Stolcis (1995), Demirdžić and Muzaferija (1995), Helf and Küster (1994), Moraga and Medina (2000), Perré and Turner (1999), Vijayan and Kallinderis (1994)). Typically, due to the conservative nature of the scheme and its ability to be implemented on either structured or unstructured meshes, it is the preferred method implemented in many industrial computational fluid dynamics codes. The accuracy of the scheme depends to a large extent on the approximation of the flux at the midpoint of the control volume face (Turkel (1985)). For many problems this approximation is crucial and the classical linear models are often inadequate, especially for anisotropic media when the anisotropy ratio is large (Jayantha and Turner (2002)).

The literature highlights only a limited number of computational schemes that accurately model transport in highly anisotropic media on completely unstructured meshes using a generalised finite volume formulation (Chow *et al.* (1996), Croft (1998), Hermeline (2000), Murthy and Mathur (1998), Demirdžić *et al.* (2000), Turner and Ferguson (1995b)). The accuracy of the existing schemes is questionable under extreme anisotropic ratios such as the one that exists in wood for permeability (of the order of 1:1000 in the radial versus longitudinal directions).

Typically, wood drying simulations require the computation of the moisture, temperature and pressure fields in a radial- longitudinal cross-section of the board for the purposes of determining the stress distribution (Ferguson and Turner (1996)). Under extreme drying conditions, the non-linear variation in the relative permeability tensors causes the transport problem to become highly orthotropic in the longitudinal direction. Most of the existing codes that are based on finite volume discretisations implemented on unstructured meshes in order to capture local heterogeneities in the wood structure, either diverge, or produce misleading results under these circumstances. This lacking of a robust numerical method for such important industrial problems provides the motivation for this research.

One can note that the use of the midpoint rule in the finite volume technique, which is described later in the text, can maintain second order accuracy only if the flux approximation at the CV face is at least second order accurate (Murthy and Mathur (1998)). The aim of this work is to propose a high order flux approximation technique that achieves this objective.

"take in Figure 1"

The numerical treatment of transport equations for orthotropic and anisotropic media using finite volume methods is a non-trivial task. In order to explain the underlying problems that occur when approximating a term of the form $(K\nabla\phi).\hat{\mathbf{n}}$ or $\nabla\phi.\mathbf{w} = \nabla\phi.(K^T\hat{\mathbf{n}})$, the following generalised form of the flux approximation at a control volume face is considered (refer Figure 1c):

$$\begin{aligned}(\nabla\phi).\mathbf{w} &= C_1 \ \nabla\phi.\mathbf{v} + \ C_2 \ (\nabla\phi.\hat{\mathbf{u}}) \\ &\simeq C_1 \ \overbrace{(\phi_N - \phi_P)}^{Primary \ \ term} + C_2 \ \overbrace{(\nabla\phi.\hat{\mathbf{u}})}^{Secondary \ \ term}\end{aligned} \tag{1}$$

where the constants C_1 and C_2 depend on the tensor K and the geometry of the control volume mesh - see Croft (1998), Mathur and Murthy (1997), Demirdžić and Muzaferija (1995), Jasak and Gosman (2000) for similar types of decompositions. The primary term is the first order Taylor approximation of $\nabla\phi.\mathbf{v}$ and the gradient required for the secondary or the cross-diffusion term can be computed using either the weighted least squares methods or the Green-Gauss gradient reconstruction (Barth (1994), Croft (1998), Jayantha and Turner (2001)). One notes however, that even if the secondary term is approximated with a high order accuracy, the error in the flux estimation is still dominated by the lower order associated with the primary term.

The above techniques have achieved considerable success for isotropic problems, however, for anisotropic problems it has been shown that such strategies can be inaccurate when the anisotropy ratio is large (Jayantha and Turner (2002)). This inaccuracy arises because the implicitly treated primary flux approximation term can be less important than the secondary term, which is usually treated explicitly in the underlying matrix system (Chow *et al.* (1996), Jayantha and Turner

(2002), Turner and Ferguson (1995a)), if the preferential direction of transport (the direction given by the vector **w** in Figure 1c) is far from the direction **v** defined by the nodes adjoining the control volume face. Hence the system matrix may not contain sufficient information of the flow. Therefore, most, if not all, of the important flux information can be lost from the matrix leading to inaccurate and misleading results. Note, however, that the problem of non-alignment of the flux vector and the vector defined by the nodes adjoining the cell face is not a particularly of anisotropic media.

The difficulty that arises concerns an accurate decomposition of the flux at the control volume faces. In order to develop a new decomposition technique, an extension of the weighted least squares approximation to reconstruct the derivatives of the function at the control volume face for determining the cross-diffusion term and an important correction to increase the accuracy of the primary term of the flux approximation will be analysed here.

One way of including the information from all the neighbours of the control volume into the resulting matrix system is to employ the control-volume finite-element method as discussed in Perré and Turner (1999) or Jayantha and Turner (2001). However, even this method becomes inaccurate for highly anisotropic transport problems, because of the linear approximation used for estimating the flux.

Bearing all of these facts in mind, higher order methods that exploit quadratic or cubic Taylor series expansions to approximate the flux at the control volume face are proposed.

The flux decomposition and subsequent approximation at the CV face presented here is novel and in most of the circumstances that were tested in this research, produces excellent results for this difficult problem. The strategy is different from previous work, (Chow *et al.* (1996), Croft (1998), Murthy and Mathur (1998), Turner and Ferguson (1995a), Jasak and Gosman (2000)) because this technique introduces a correction for the primary term of the Eq. (1). Furthermore, the improved least squares technique discussed here produces not only derivatives of the function, but also the function value at the required point on the control volume face.

The overall methodology is summarised by the following flux decomposition formula:

$$\begin{aligned}(\nabla\phi).\mathbf{w} &= C_1 \ \nabla\phi.\mathbf{v} + \ C_2 \ (\nabla\phi.\hat{\mathbf{u}}) \\ &\simeq C_1 \ \overbrace{(\phi_N - \phi_P) + \epsilon}^{Primary \quad term} \ + \ C_2 \ \overbrace{(\nabla\phi.\hat{\mathbf{u}})}^{Secondary \quad term}\end{aligned} \tag{2}$$

The estimation of the parameter ϵ and the gradient, $\nabla\phi$, at the control volume faces, using an improved least squares function reconstruction provides an excellent approximation that increases the overall order of the estimation of the flux to as high as cubic. This strategy increases the accuracy of the primary term as

well as the secondary or cross diffusion term, therefore, the finite volume scheme maintains second order spatial accuracy. However, there still remains some problems for which this strategy does not provide good results, for example, under extreme cases of anisotropy ratios like 1 : 10000, because of the explicit treatment of the secondary term and the correction in the control volume solution process. The authors are presently working on a new technique that will address this problem.

To assess the accuracy and efficiency of the proposed schemes the following two-dimensional anisotropic transport problem for a finite rectangular domain is considered:

$$\nabla.(K\nabla\phi) = \rho\, C_p \frac{\partial\phi}{\partial t};\;\; 0 \le x \le L,\;\; 0 \le y \le M;\;\; t > 0 \tag{3}$$

where $K = \begin{pmatrix} k_{xx} & k_{xy} \\ k_{yx} & k_{yy} \end{pmatrix}$.

$$(K\nabla\phi).\hat{\mathbf{n}}_b = h_b(\phi_s - \phi);\quad \text{at boundary } S_b,\;\; t > 0$$

where $\hat{\mathbf{n}}_b$ is outward unit normal vector at boundary b, and initially

$$\phi(x, y, 0) = \phi_0;\quad 0 < x < L;\quad 0 < y < M,$$

and note that the coefficients k_{xy} and k_{yx} are zero for the orthotropic case.

Exact solutions for the orthotropic case, and the numerical results computed on very fine meshes for the anisotropic cases where analytical solutions are unavailable, will be used to assess the accuracy of the new scheme.

This paper is organised as follows. In the next section the theoretical solution used to benchmark the new numerical scheme is presented. Thereafter the complete analysis of the finite volume technique, together with the flux approximation are given. Then there follows a discussion of the numerical simulation results offered by the new finite volume methodology. It can be observed that the new method produces an excellent fit with analytical solutions obtained by using the methods in Özişik (1980) for all orthotropic cases tested. The conclusions of the work are summarised in the final section of the paper.

Theoretical Solution

For the purposes of assessing the accuracy of the proposed finite volume scheme, case studies will compare the simulation results with analytical solutions of Eq. (3), for the orthotropic case (i.e., when $k_{xy} = 0$ and $k_{yx} = 0$). The system (3) is transformed into dimensionless form (Özişik (1980)) by using the following

parameters:

$$X = \frac{x}{L}, \quad Y = \frac{y}{M}, \quad \tau = \frac{k_{xx}t}{\rho C_p L^2}, \quad Bi_1 = \frac{h_1 M}{k_{yy}},$$
$$Bi_2 = \frac{h_2 L}{k_{xx}}, \quad Bi_3 = \frac{h_3 M}{k_{yy}}, \quad Bi_4 = \frac{h_4 L}{k_{xx}},$$
$$\Theta(X,Y,\tau) = \frac{(\phi - \phi_s)}{(\phi_0 - \phi_s)}; 0 \le \Theta \le 1$$

to obtain

$$\frac{\partial^2\Theta}{\partial X^2} + \frac{k_{yy}L^2}{k_{xx}M^2}\frac{\partial^2\Theta}{\partial Y^2} = \frac{\partial\Theta}{\partial\tau}; \quad 0 \le X \le 1, \;\; 0 \le Y \le 1, \;\; \tau > 0 \tag{4}$$

with boundary conditions

$$-\frac{\partial\Theta}{\partial X} + Bi_4\Theta = 0; \;\; X = 0, \qquad \frac{\partial\Theta}{\partial X} + Bi_2\Theta = 0; \;\; X = 1,$$
$$-\frac{\partial\Theta}{\partial Y} + Bi_1\Theta = 0; \;\; Y = 0 \quad \text{and} \quad \frac{\partial\Theta}{\partial Y} + Bi_3\Theta = 0; \;\; Y = 1, \text{ for } \tau > 0$$

and initial condition $\Theta(X,Y,0) = 1$, for $0 < X < 1, \;\; 0 < Y < 1$. Assuming a separation in the form $\Theta(X,Y,\tau) = \Theta_1(X,\tau)\Theta_2(Y,\tau)$ it can be shown that

$$\Theta_1(X,\tau) = \sum_{m=1}^{\infty} \frac{\psi(\beta_m, X)}{N_x(\beta_m)}(\sin\beta_m - \frac{Bi_4}{\beta_m}\cos\beta_m + \frac{Bi_4}{\beta_m})e^{-\beta_m^2\tau}$$

where

$$\psi(\beta_m, X) = \beta_m\cos(\beta_m X) + Bi_4\sin(\beta_m X) \text{ for } 0 < X < 1;$$
$$(\beta_m^2 - Bi_2 Bi_4)\tan\beta_m = (Bi_2 + Bi_4)\beta_m;$$
$$N_x(\beta_m) = \frac{1}{2}[(\beta_m^2 + Bi_4^2)(1 + \frac{Bi_2}{\beta_m^2 + Bi_2^2}) + Bi_4]$$

and

$$\Theta_2(Y,\tau) = \sum_{n=1}^{\infty} \frac{\chi(\mu_n, Y)}{N_y(\mu_n)}(\sin\mu_n - \frac{Bi_1}{\mu_n}\cos\mu_n + \frac{Bi_1}{\mu_n})e^{-\mu_n^2 r^2\tau}$$

where $r^2 = \frac{k_{yy}}{k_{xx}}\frac{L^2}{M^2}$, and

$$\chi(\mu_n, Y) = \mu_n\cos(\mu_n Y) + Bi_1\sin(\mu_n Y) \text{ for } 0 < Y < 1;$$
$$(\mu_n^2 - Bi_1 Bi_3)\tan\mu_n = (Bi_1 + Bi_3)\mu_n; \tag{5}$$
$$N_y(\mu_n) = \frac{1}{2}[(\mu_n^2 + Bi_1^2)(1 + \frac{Bi_3}{\mu_n^2 + Bi_3^2}) + Bi_1].$$

Using the above equations, the analytical solution of Eq. (3) for the orthotropic case can be obtained as

$$\phi(x,y,t) = \phi_s + \Theta_1(X,\tau)\Theta_2(Y,\tau)(\phi_0 - \phi_s) \;\; \text{for} \;\; 0 < x < L, \;\; 0 < y < M, \;\; t > 0.$$

Finite volume technique

The finite volume technique (Patankar (1980) and Turkel (1985)) concerns the direct discretisation in physical space of the integral formulation of a given conservation law. The method enables an arbitrary mesh to be employed for the computations and a variety of options exist for the definition of the control volumes around which the conservation law is expressed. It should be noted however that the sum of all control volumes must cover the entire computational domain and the control volumes cannot overlap without having common surfaces.

The possibilities of modifying the shape and location of the control volumes associated with a given mesh point, together with the complete flexibility in evaluating the fluxes through the control volume faces make the method a popular choice for use in a variety of applications in science, engineering and technology. The most important property of the method is the conservative nature of the scheme, basic quantities such as mass, momentum and energy remain conserved at the discrete level.

"take in Figure 2"

Figure 2 exhibits four background finite element triangular meshes generated using EasyMesh developed by Niceno. The control volumes are constructed around the vertices of the triangles by joining the centroids of adjacent elements. These particular meshes have been chosen in order to demonstrate the complete flexibility of the new flux approximation scheme proposed in this work.

Figure 1 exhibits typical control volumes for a two-dimensional framework within an unstructured mesh of the vertex-centered control volume approach. The control volume with the centroid point, P, has neighbouring nodes, N_k, $k = 1, 2, .., p$.

The discretised form of the differential Eq. (3) is derived by integrating the equation over the control volume. The use of the divergence theorem in the plane leads to

$$\rho C_p \frac{d\overline{\phi}}{dt} - \frac{1}{\delta V_P} \oint_{\Gamma_P} (K \nabla \phi).\hat{\mathbf{n}} d\Gamma = 0 \tag{6}$$

where

$$\overline{\phi} = \frac{1}{\delta V_P} \int_{\delta V_P} \phi dV, \tag{7}$$

is the average of ϕ in a control volume. As there is no approximation made to this point, the Eq. (6) together with (7) is exact (Turkel (1985)). Discretising Eq. (6) one can obtain

$$\rho C_p \frac{d\overline{\phi}}{dt} - \sum_{k=1}^{Np} \{(K \nabla \phi).\hat{\mathbf{n}}\}_{F_k} A_k \simeq 0, \tag{8}$$

which is second order in space if the term $(K\nabla\phi).\hat{\mathbf{n}}$ is accurately evaluated at the midpoint of the control volume face.

Assuming that ϕ_P represents the averaged value of ϕ over δV_P and considering the time integral from $n\delta t$ to $(n+1)\delta t$, the discrete form of Eq. (8) can be written as

$$\begin{aligned}\rho\, C_p \frac{\delta V_P}{\delta t}(\phi_P^{(n+1)} - \phi_P^{(n)}) \\ -\{\lambda \sum_{k=1}^{Np} \{(K\nabla\phi).\hat{\mathbf{n}}\}_{F_k}^{(n+1)} A_k + (1-\lambda) \sum_{k=1}^{Np} \{(K\nabla\phi).\hat{\mathbf{n}}\}_{F_k}^{(n)} A_k\} \simeq 0.\end{aligned} \tag{9}$$

The term $(K\nabla\phi).\hat{\mathbf{n}}$ can be expressed as $\nabla\phi.(K^T\hat{\mathbf{n}})$ and hence, the above equation can be rewritten as

$$\begin{aligned}\rho\, C_p \frac{\delta V_P}{\delta t}(\phi_P^{(n+1)} - \phi_P^{(n)}) \\ -\{\lambda \sum_{k=1}^{Np} \{(\nabla\phi).\mathbf{w}\}_{F_k}^{(n+1)} A_k + (1-\lambda) \sum_{k=1}^{Np} \{(\nabla\phi).\mathbf{w}\}_{F_k}^{(n)} A_k\} \simeq 0\end{aligned} \tag{10}$$

where $\mathbf{w} = K^T\hat{\mathbf{n}}$. The parameter $\lambda = 1$ gives a fully implicit scheme, $\lambda = 0$ leads to a fully explicit scheme and $\lambda = \frac{1}{2}$ provides a second order scheme in time. The parameter λ is set to 1 for this study.

The accuracy of the scheme hinges around the approximation of the flux term at the CV face. The discrete form (10) allows a first order accuracy in time and a second order approximation in space when the flux approximation at the midpoint of the CV faces is at least second order accurate (Murthy and Mathur (1998)).

Flux approximation using decomposed vectors (FADV)

Figure 1b shows a control volume face in a two-dimensional framework. The unit vectors $\hat{\mathbf{n}}_k$ and $\hat{\mathbf{u}}_k$ are perpendicular to each other, and the vector joining the points P and N_k, $\mathbf{v}_k$, is perpendicular to $\hat{\mathbf{t}}_k$. The vector $\mathbf{w}_k = K^T\hat{\mathbf{n}}_k$ can be decomposed as follows. Note that subscript k is suppressed in the following equations.

The two vector equations $\mathbf{v} = (\mathbf{v}.\hat{\mathbf{u}})\hat{\mathbf{u}} + (\mathbf{v}.\hat{\mathbf{n}})\hat{\mathbf{n}}$ and $\mathbf{w} = (\mathbf{w}.\hat{\mathbf{u}})\hat{\mathbf{u}} + (\mathbf{w}.\hat{\mathbf{n}})\hat{\mathbf{n}}$ give the following formulae:

$$\hat{\mathbf{n}} = \frac{\mathbf{v} - (\mathbf{v}.\hat{\mathbf{u}})\hat{\mathbf{u}}}{\mathbf{v}.\hat{\mathbf{n}}} \tag{11}$$

and

$$\begin{aligned}\mathbf{w} &= (\mathbf{w}.\hat{\mathbf{u}})\hat{\mathbf{u}} + (\mathbf{w}.\hat{\mathbf{n}})\frac{\mathbf{v} - (\mathbf{v}.\hat{\mathbf{u}})\hat{\mathbf{u}}}{\mathbf{v}.\hat{\mathbf{n}}} \\ &= \frac{\mathbf{w}.\hat{\mathbf{n}}}{\mathbf{v}.\hat{\mathbf{n}}}\mathbf{v} + \{\mathbf{w}.\hat{\mathbf{u}} - \mathbf{w}.\hat{\mathbf{n}}\frac{\mathbf{v}.\hat{\mathbf{u}}}{\mathbf{v}.\hat{\mathbf{n}}}\}\hat{\mathbf{u}}.\end{aligned} \tag{12}$$

Therefore an expression for $\nabla\phi.\mathbf{w} = \nabla\phi.(K^T\hat{\mathbf{n}})$ can be written as

$$\nabla\phi.\mathbf{w} = \frac{\mathbf{w}.\hat{\mathbf{n}}}{\mathbf{v}.\hat{\mathbf{n}}}\nabla\phi.\mathbf{v} + \{\mathbf{w}.\hat{\mathbf{u}} - \mathbf{w}.\hat{\mathbf{n}}\frac{\mathbf{v}.\hat{\mathbf{u}}}{\mathbf{v}.\hat{\mathbf{n}}}\}\nabla\phi.\hat{\mathbf{u}}. \tag{13}$$

which is valid for the two-dimensional case. In order to estimate the primary term $\nabla\phi.\mathbf{v}$, consider the following analysis.

"take in Figure 3"

Write the vectors emanating from the point F, the midpoint of the control volume face, to the points P and N as (see Figure 3a) $\delta\underline{\mathrm{x}}^- = (\delta x_1^-, \delta x_2^-)$ and $\delta\underline{\mathrm{x}}^+ = (\delta x_1^+, \delta x_2^+)$ respectively. Consider Taylor expansions of the function ϕ:

$$\phi(\underline{\mathrm{x}}_F + \delta\underline{\mathrm{x}}^+) = \sum_{k=0}^{m}\frac{1}{k!}(\delta\underline{\mathrm{x}}^+.\nabla)^k\phi(\underline{\mathrm{x}}_F) + R^+ \tag{14}$$

and

$$\phi(\underline{\mathrm{x}}_F + \delta\underline{\mathrm{x}}^-) = \sum_{k=0}^{m}\frac{1}{k!}(\delta\underline{\mathrm{x}}^-.\nabla)^k\phi(\underline{\mathrm{x}}_F) + R^- \tag{15}$$

where the remainder R has the *Lagrange form* and for example,

$$R^+ = \frac{1}{(m+1)!}(\delta\underline{\mathrm{x}}^+.\nabla)^{(m+1)}\phi(\underline{\mathrm{x}}_F + \theta\delta\underline{\mathrm{x}}^+); \quad 0 \le \theta \le 1.$$

Subtracting (15) from (14) and assuming that $R^+ - R^- \simeq 0$ (*i.e.*, negligible) the following expression for $(\nabla\phi)_F.\mathbf{v}$ can be obtained;

$$(\nabla\phi)_F.\mathbf{v} \simeq (\phi_N - \phi_P) - \epsilon_{np} \tag{16}$$

where

$$\epsilon_{np} \simeq \sum_{k=2}^{m}\frac{1}{k!}\{(\delta\underline{\mathrm{x}}^+.\nabla)^k - (\delta\underline{\mathrm{x}}^-.\nabla)^k\}\phi(\underline{\mathrm{x}}_F). \tag{17}$$

It is possible to assume that $\epsilon_{np} \simeq 0$ for fine meshes, however, it may not be suitable to use fine meshes because this requires more storage and memory requirements for the numerical simulations. Substitution of Eq. (16) into (13) gives the following expression for the flux at the control volume face:

$$\begin{aligned}\{(K\nabla\phi).\hat{\mathbf{n}}\}_{F_k}^{(n+1)} \simeq & \frac{\mathbf{w}.\hat{\mathbf{n}}}{\mathbf{v}.\hat{\mathbf{n}}}(\phi_{N_k}^{(n+1)} - \phi_P^{(n+1)}) \\ & + \{\mathbf{w}.\hat{\mathbf{u}} - \mathbf{w}.\hat{\mathbf{n}}\frac{\mathbf{v}.\hat{\mathbf{u}}}{\mathbf{v}.\hat{\mathbf{n}}}\}(\nabla\phi.\hat{\mathbf{u}})_{F_k}^{(n+1)} - \frac{\mathbf{w}.\hat{\mathbf{n}}}{\mathbf{v}.\hat{\mathbf{n}}}(\epsilon_{np})_{F_k}^{(n+1)}.\end{aligned} \tag{18}$$

To complete the flux approximation, $\nabla\phi.\hat{\mathbf{u}}$ and ϵ_{np} must be evaluated at the control volume faces k. The following section describes approximation techniques to evaluate the required terms using the function values at the n^{th} time step since the function values are not readily available at time step $n+1$.

Improved least squares gradient reconstruction (*ILSGR)*

The Taylor series expansion has been used to estimate the functions of interest by Jasak and Gosman (2000) in order to analyse errors in regular finite volume techniques. In this article, the Taylor series expansion of the function is considered to estimate the derivatives of the function and to use those derivatives to estimate the correction term ϵ_{np} which contributes the finite volume discretisation - see Eqs. (2), (16) and (17) for the required correction term. Consider the truncated Taylor expansion of the function ϕ:

$$\phi(\underline{\mathrm{x}}_F + \delta\underline{\mathrm{x}}_d) \simeq \sum_{k=0}^{m} \frac{1}{k!}(\delta\underline{\mathrm{x}}_d.\nabla)^k \phi(\underline{\mathrm{x}}_F) \tag{19}$$

Writing Eq. (19) for each node, $d = 1, 2, ..., r$, see Figure 3c for the nodes indicated by small circles, connected to the point F, the following over-determined system of equations is obtained, (for $m = 3$) :

$$\begin{pmatrix} 1 & \Delta x_1 & \Delta y_1 & ... & \frac{\Delta x_1^3}{6} & \frac{\Delta y_1^3}{6} & \frac{\Delta x_1^2 \Delta y_1}{2} & \frac{\Delta x_1 \Delta y_1^2}{2} \\ 1 & \Delta x_2 & \Delta y_2 & ... & \frac{\Delta x_2^3}{6} & \frac{\Delta y_2^3}{6} & \frac{\Delta x_2^2 \Delta y_2}{2} & \frac{\Delta x_2 \Delta y_2^2}{2} \\ . & . & . & & . & . & . & . \\ . & . & . & & . & . & . & . \\ . & . & . & & . & . & . & . \\ 1 & \Delta x_r & \Delta y_r & ... & \frac{\Delta x_r^3}{6} & \frac{\Delta y_r^3}{6} & \frac{\Delta x_r^2 \Delta y_r}{2} & \frac{\Delta x_r \Delta y_r^2}{2} \end{pmatrix} \begin{pmatrix} \phi_F \\ \frac{\partial \phi}{\partial x}_F \\ \frac{\partial \phi}{\partial y}_F \\ . \\ . \\ \frac{\partial^3 \phi}{\partial x \partial y^2}_F \end{pmatrix} = \begin{pmatrix} \phi_1 \\ \phi_2 \\ . \\ . \\ . \\ \phi_r \end{pmatrix} \tag{20}$$

which can be written as

$$A\mathbf{X} = \mathbf{B}.$$

At a boundary control face, see Figure 3b, an equation related to the boundary conditions is added to the above system. For example, for the face F shown in Figure 3b, the equation,

$$k_{xx}\frac{\partial \phi}{\partial x}_F + k_{xy}\frac{\partial \phi}{\partial y}_F = h_w(\phi_F - \phi_w),$$

$$\text{or} \quad h_w\phi_F - k_{xx}\frac{\partial \phi}{\partial x}_F - k_{xy}\frac{\partial \phi}{\partial y}_F = h_w\phi_w,$$

is also inserted to the system of equations given by Eq. (20).

The components that minimise $||A\mathbf{X}-\mathbf{B}||^2$ in the least squares sense with respect to a weighted inner product on $\mathbb{R}^r$ can be determined by multiplying the above system by $W_{r\times r} = Diag(w_k)$ and A^T, to arrive at the normal equations

$$(A^T W A)\,\mathbf{X} = (A^T W \mathbf{B}). \tag{21}$$

Note that the weight coefficients, w_k's, are chosen so that more importance is given to the directions that are the closest neighbours of the point F as opposed to the nodes that are further away from the point F, and $w_k = ||\mathbf{v}_k||^{-c}; \quad c = 0, 1, 2$ is used for the numerical simulations. Solving the above system, it is possible to find the function value and the first, second and third derivatives accurately at the point F on the CV face and therefore the terms $\nabla\phi.\hat{\mathbf{u}}$ and ϵ_{np} required for Eq. (18) can be estimated.

It should be noted that the technique discussed here estimates the function value on the control volume face also with a high accuracy. The typical least-squares gradient reconstruction technique found in Barth (1994), Ilinca *et al.* (2000), Jayantha and Turner (2001,2002) or Ollivier-Gooch (1996) only approximates the derivatives of the function.

"take in Table 1"

The special cases of the above technique as shown in Table 1b are considered to approximate the terms $\nabla\phi.\hat{\mathbf{u}}$ and ϵ_{np}. For all of these least squares methods the closest nodes to the midpoint F (see Figure 3c) on each control volume face are used. Although it was found that the closest node points for each face is sufficient for most unstructured meshes, more node points were used for the highly distorted mesh to cover every gradient direction around each control volume face. Those additional node points are chosen to ensure that every node connected to the node points P, N, A and B were included for each face.

Numerical simulations

To test the flux approximation techniques discussed in the above sections, a wood like material is used with the physical properties: $L = 0.1m$, $M = 0.04m$, $h_b = 10W/m^2/K$, $\rho = 600kg/m^3$ and $C_p = 1.6886 \times 10^3 J/kg/K$, with $\phi_0 = 30^0C$ and $\phi_s = 140^0C$. The values given in Table 1a are used for the tensor K to obtain the results presented here. The time step, δt, used for the simulations is one second and the results shown are obtained after 1000 seconds. The meshes shown in Figure 2 are used to implement the flux decomposition techniques.

Throughout the tests, $c = 2$ is used for the weights $w_k = ||\mathbf{v}_k||^{-c}$. The results are not accurate for $c = 0$ and $c = 1$, when the distorted mesh shown in Figure 2d is used. However, $c = 0$, $c = 1$ and $c = 2$ provide accurate results on other regular unstructured finite-volume meshes.

At the initial stage of the numerical procedure, the matrix A, the diagonal entries of W, the decomposed form the matrix $A^T W A$ in Eq. (21) and the matrix $A^T W$ are stored for each control volume face because those matrices depend only on geometrical terms and constant parameters. During the processing one can form $A^T W \underline{\mathrm{B}}$ and process forward and backward substitution to obtain the least squares solution vector $\mathbf{X}$ at each time step. The vector $\mathbf{X}$ provides the function

value and its derivatives at each control volume face for each time step during the control volume solution process. This strategy is used for every method discussed above.

Each method produces the gradient $\nabla\phi.\hat{\mathbf{u}}$ on the midpoint of each control volume face and enables ϵ_{np} to be evaluated. Therefore the flux through the CV faces can be calculated using Eq. (18) and hence Eq. (10), with the choice $\lambda = 1$, produces a system of linear equations when every node point on a mesh is visited. The resulting system is solved using the *BiCGSTAB* iteration technique (van der Vorst (1992) and Turner and Perré (1996)) for each time level to obtain the final result.

The terms $\nabla\phi.\hat{\mathbf{u}}$ and ϵ_{np} are treated explicitly in the finite volume formulation, however, for some meshes and very large anisotropy ratios this approach may not be sufficient. The authors are presently working on the implicit treatment of the complete flux decomposition.

"take in Table 2"

The total number of iterations (T.I.), maximum error (M.E.), and root mean square error (*RMSE*) are tabulated in Table 2 for each mesh and each method for the cases 1 and 2 where the exact solutions are found using the method described earlier in this article. The *RMSE* is calculated using the formula

$$RMSE = \sqrt{\frac{\sum_{k=1}^{M_n} \left(\phi_{k,exact} - \phi_k\right)^2}{\sum_{k=1}^{M_n} \left(\phi_{k,exact}\right)^2}} \tag{22}$$

where ϕ_k is the value of the variable at node point k, $\phi_{k,exact}$ is the exact solution at the same point, and M_n is the number of node points on a mesh.

A comparison of the contour plots for cases 1 and 2 obtained on the distorted mesh, Figure 2d, is shown in Figure 4. Figure 5 exhibits the results for the cases 4 and 5 on the coarse mesh, Figure 2c. Figures 6 and 7 depict comparisons of the results for the same mesh for cases 1 and 2, respectively. Figure 8 shows the numerical results for the anisotropic cases 3 and 6, while Figures 9-11 show the results for the anisotropic cases 7 and 8.

Note that the attraction for using the orthotropic model, in cases 1,2,4 and 5, is that exact solutions are available for an accuracy check on the proposed flux approximation scheme, see Table 2.

"take in Figure 4"
"take in Figure 5"
"take in Figure 6"
"take in Figure 7"

An important observation from Table 2, and Figures 4-7 indicates that the *ILSGR*3 technique, which uses the new scheme with a high order (cubic) least squares approximation, produces accurate results for each mesh, including the distorted mesh shown in Figure 2d, for all of the orthotropic cases tested. One can see from Table 2 (*RMSE* and M.E. columns) that the different anisotropy ratios can influence the accuracy of the *ILSGR*2 technique, whereas the accuracy of the *ILSGR*3 technique remains unaffected.

Results have also been computed for the orthotropic cases where $k_{xx} : k_{yy} = 1 : 10, \quad 1 : 100, \quad 10 : 1, \quad 100 : 1$ using the *ILSGR*3 technique and excellent agreement with the exact solutions was found on all of the meshes, and therefore those results were not exhibited here. Note that these case studies are typical scenarios that arise in wood drying simulation and represent real two-dimensional tests for the numerical scheme, since the strongly orthotropic case is nearly one-dimensional.

Figure 4 shows a close agreement between the exact solutions and the results provided by *ILSGR*3 on the distorted mesh, Figure 2d. The true symmetry of the solutions are slightly concealed in these figures due to the mesh irregularity and limitations of the plotting software used. In fact, this behaviour is evident also in the exact solutions (Figure 4a and 4c), again due to the interpolation method used in the plotting software.

Figure 5 exhibits the results obtained for the cases 4 and 5, where the exact solutions are compared to the results obtained using *ILSGR*3 and *ILSGR*4. These cases use lower anisotropy ratios to emphasise the two-dimensional transport process. One can see that when the primary correction term is included the *ILSGR*3 scheme is able to capture the exact results, and that *ILSGR*4 fails even though the cross diffusion term is estimated using a cubic approximation. Further evidence of these facts can be seen in Table 2, where the *ILSGR*2-3 schemes generate the lowest *RMSE*. It also can be seen from the Table that the *ILSGR*4 scheme did not converge for cases 1 and 5, whereas it did converge for cases 2 and 4.

It is possible to see from Figure 6 that *ILSGR*1, *ILSGR*4 and the hybrid technique produce inaccurate results for Case 1, whereas *ILSGR*2 and *ILSGR*3 produce results that well match the exact solution. However, according to Figure 7, while the hybrid technique provides a reasonable result for Case 2, *ILSGR*1, *ILSGR*2 and *ILSGR*4 fail to produce accurate results and again *ILSGR*3 produces good agreement with the exact solution. In fact, Figures 6 and 7 identify the differences, in terms of the accuracy of the different techniques, between the cases 1 and 2, which can be considered as nearly one-dimensional. It can be concluded from these results that the combination of the geometry of the solution domain and the direction of anisotropy can affect the accuracy of the numerical solution technique.

The results shown in Figures 6 and 7 highlight that *ILSGR*1, *ILSGR*2 and the hybrid method provide poor accuracy for the strongly orthotropic cases. It is

worthwhile to note that a significant error arises in $ILSGR4$ when the correction ϵ_{np}, which plays a major role in increasing the order of the primary term in the flux approximation, is neglected from $ILSGR3$. These finding are an important conclusion to be drawn from this research, especially for the development of accurate wood drying simulators.

Since the $ILSGR3$ technique provides very accurate results on all of the unstructured meshes investigated here for the orthotropic cases, this method was used on the fine mesh shown in Figure 2a to produce the benchmarking results for the anisotropic problems discussed next in cases 3 and 6-8 for assessing the results computed using the very coarse mesh.

"take in Figure 8"
"take in Figure 9"
"take in Figure 10"
"take in Figure 11"

Figure 8 provides the results for cases 3 and 6, which are anisotropic problems. Figures 8a and 8c depict the results using $ILSGR3$ on a very fine unstructured mesh. Figures 8b and 8d again show that the $ILSGR3$ method used on a very coarse mesh provides good agreement with the benchmark solutions, due to the accuracy of the gradient approximation used.

Figures 9, 10 and 11 exhibit the results for cases 7 and 8, which are strongly anisotropic problems. The results for case 7, shown here as contour plots in Figure 9 and as a cross-sectional view in Figure 10, again show that the $ILSGR2$-3 techniques match the benchmark solution well. Clearly, omitting the correction term ($ILSGR4$) produces an inconsistent behaviour in the solution and the results of the first order methods ($ILSGR1$ and hybrid method) are far from the benchmark solution. Similar conclusions can be drawn from the results presented for case 8 in Figure 11.

Some final reflections from Table 2 concerning the computational performance of each scheme indicate that the hybrid technique has used more solver iterations than $ILSGR3$ to produce the results and $ILSGR3$ always produces more accurate results than the hybrid technique. It can be seen that all of the $ILSGR$ techniques use approximately the same number of solver iterations, however the hybrid technique always uses more. While the hybrid technique, which is a fully implicit scheme, fails to produce accurate results, $ILSGR3$, which is not a fully implicit scheme, always produces excellent results due to its higher order accuracy of the flux approximation.

All of the results shown in this section support the conclusion that $ILSGR3$ is the best technique amongst the methods considered here for solving transport in both anisotropic media and strongly orthotropic media, including transport problems that involve large anisotropy ratios ranging from $1:1000$ or $1000:1$. Note however, that $ILSGR2$, although not always as accurate as $ILSGR3$, can

be used to solve such problems and given that it requires less computational overhead than $ILSGR3$, it may well be the favoured solution strategy.

Conclusions

In this work a highly accurate flux approximation technique appropriate for use in simulating transport in strongly orthotropic and anisotropic media in two dimensions using a finite volume method implemented on unstructured meshes was presented in detail. The results offered by this new method highlight the possibilities of the proposed scheme. The computational cost of the scheme is minimal when one considers the excellent comparison with the analytical results.

In summary, the finite volume technique discussed here has combined a new flux decomposition with the use of a high order least squares approximation technique, which estimates both the cross-diffusion term and the correction ϵ_{np} for the primary term, to increase the overall accuracy of the flux approximation at the CV face. Such a strategy ensures that the finite volume method achieves second order spatial accuracy.

It is felt that the method outlined in this research represents an original and important contribution to the field of finite volume techniques for solving transport problems in highly orthotropic and anisotropic media. The next stage of the research is to analyse its performance when implemented in a drying simulator and thereafter, to extend this technique to a three-dimensional framework.

Acknowledgments
Both authors would like to thank the anonymous reviewer for the many fruitful comments that improved the presentation of the manuscript. The first author wishes to acknowledge the financial support provided by the Queensland University of Technology under the IPRS scholarship program and the leave granted for the studies from the University of Ruhuna, Sri Lanka, where he is affiliated as a Lecturer.

References

[1] Bailey, C., Taylor, G. A., Cross, M. and Chow, P. (1999), "Discretisation Procedures for multi-Physics Phenomena", Journal of Computational and Applied Mathematics, Vol. 103, pp. 3-17.

[2] Barth, T. J. (1994), "Aspects of Unstructured Grids and Finite-Volume Solvers for the Euler and Navier-Stokes Equations", in: Lecture Notes Presented at the VKI Lecture Series 1994-05, Feb.

[3] Chow, P., Cross, M. and Pericleous, K. (1996), "A Natural Extension of the Conventional Finite Volume Method into Polygonal Unstructured Meshes for CFD Application", Applied Mathematical Modelling, Vol. 20, pp. 170-183.

[4] Croft, N.(1998), "Unstructured Mesh - Finite Volume Algorithms for Swirling, Turbulent, Reacting Flows", PhD. Thesis, University of Greenwich, London, UK.

[5] Davidson, L. and Stolcis, L. (1995), "An Efficient and Stable Solution Procedure of Turbulent Flow on General Unstructured Meshes using Transport Turbulence Models", in: AIAA - 33rd Aerospace Sciences Meeting and Exhibit, Reno, NV, US, AIAA-95-0342.

[6] Demirdžić, I and Muzaferija, S. (1995), "Numerical Method for Coupled Fluid Flow, heat Transfer and Stress Analysis using Unstructured Moving Meshes with Cells of Arbitrary Topology", Computer Methods in Applied Mechanics and Engineering, Vol. 125, pp. 235-255.

[7] Demirdžić, Horman, I. and Martinović, D., (2000), "Finite Volume Analysis of Stress and Deformation in Hygro-Thermo-Elastic Orthotropic Body", Computer Methods in Applied Mechanics and Engineering, Vol. 190, pp. 1221-1232.

[8] Ferguson, W. J. and Turner, I. W., (1996) A Control Volume Finite Element Numerical Simulation of the Drying of Spruce, Journal of Computational Physics, Vol. 125, pp. 59- (1996).

[9] Helf, C. and Küster, U. (1994), "A Finite Volume Method with Arbitrary Polygonal Control Volumes and High Order Reconstruction for the Euler Equations", CFD Conference, European Community on Computational methods in Applied Sciences - 94, John Wiley & Sons, Ltd.

[10] Hermeline, F. (2000), "A Finite Volume Method for the Approximation of Diffusion Operators on Distorted Meshes", Journal of Computational Physics, Vol. 160, pp. 481-499.

[11] Ilinca, C., Zhang, X. D., Trépanier, J. -Y. and Camarero, R. (2000), "A Comparison of Three Error Estimation Techniques for Finite-Volume Solutions of Compressible Flows", Computer Methods in Applied Mechanics and Engineering, Vol. 189, pp. 1277-1294.

[12] Jasak, H. and Gosman, A. D. (2000), "Automatic Resolution Control for the Finite-Volume Method, Part 1: A-Posteriori Error Estimates", Numerical Heat Transfer, Part B: Fundamentals, Vol. 38, pp. 237-256.

[13] Jayantha, P. A. and Turner, I. W. (2001) "A Comparison of Gradient Approximations for use in Finite Volume Computational Models for Two-Dimensional Diffusion Equations", Numerical Heat Transfer, Part B: Fundamentals, Vol. 40(5), pp. 367-390.

[14] Jayantha, P. A. and Turner, I. W. (2002), (to appear) "Generalised Finite Volume Strategies for Simulating Transport in Strongly Orthotropic Porous Media", Proceedings - The 10th Biennial Computational Techniques and Applications Conference, University of Queensland, Australian & New Zealand Industrial and Applied Mathematics Journal.

[15] Mathur, S. R. and Murthy, J. Y. (1997), "A Pressure-Based Methods for Unstructured Meshes", Numerical Heat Transfer Part B: Fundamentals Vol. 31, pp. 195-215.

[16] Moraga, N. O. and Medina, E. E. (2000), "Conjugate Forced Convection and Heat Conduction with Freezing of Water Content in a Plate Shaped Food", International Journal of Heat and Mass Transfer, Vol. 43, pp. 53-67.

[17] Murthy, J. Y. and Mathur, S. R. (1998), "Computation of Anisotropic Conduction using Unstructured Meshes", Journal of Heat Transfer, Vol. 120, pp. 583-591.

[18] Niceno, B., "EasyMesh" (Version 1.4), freely available mesh generator on the web Site: `http://www-dinma.univ.trieste.it/~nirftc/research/easymesh/`.

[19] Ollivier-Gooch, C. F. (1996), "A New Class of ENO Schemes Based on Unlimited Data-Dependent Least-Squares Reconstruction", in: AIAA - 34th Aerospace Sciences Meeting and Exhibit, Reno, NV, US, AIAA-96-0887.

[20] Özişik, M. N. (1980), Heat Conduction, 1st ed., Wiley, New York.

[21] Patankar, S. V. (1980), Numerical Heat Transfer and Fluid Flow, Hemisphere Publishing Corporation.

[22] Perré, P. and Turner, I. (1999), "TransPore: A Generic Heat and Mass Transfer Computational Model for Understanding and Visualising The Drying Of Porous Media", Invited paper, Drying Technology Journal, Vol. 17(7), 1273-1289.

[23] Turkel, E. (1985), "Accuracy of Schemes with Nonuniform Meshes for Compressible Fluid Flows", Institute for Computer Applications in Science and Engineering, Report No. 85-43, National Aeronautics Space Administration, Virginia.

[24] Turner, I. W. and Ferguson, W. J. (1995a), "An unstructured mesh cell-centered control volume method for simulating heat and mass transfer in porous media: Application to softwood drying, Part I: The isotropic model", Applied Mathematical Modelling, Vol. 19, pp. 654-667.

[25] Turner, I. W. and Ferguson, W. J. (1995b), "An unstructured mesh cell-centered control volume method for simulating heat and mass transfer in porous media: Application to softwood drying-Part I: The anisotropic model", Applied Mathematical Modelling, Vol. 19, pp. 668-674.

[26] Turner, I. and Perré, P. (1996), "A Synopsis of the Strategies and Efficient Resolution Techniques used for Modelling and Numerically Simulating the Drying Process", in I. Turner A. S. Mujumdar (Eds.), Mathematical Modeling and Numerical Techniques in Drying Technology, Chap. 1, Marcel Dekker, Inc. New York,

[27] van der Vorst, H.A. (1992), "BI-CGSTAB: A Fast and Smoothly Converging Variant of BI-CG for the Solutions of Nonsymmetric Linear Systems", SIAM J. Sci. Stat. Comput., Vol 13, No. 2, pp. 631-644.

[28] Vijayan, P. and Kallinders Y., (1994), "A 3D Finite-Volume Scheme for the Euler Equations on Adaptive Tetrahedral Grids", Journal of Computational Physics, Vol. 133, pp. 249-267.

(a)	Case 1	Case 2	Case 3	Case 4	Case 5	Case 6	Case 7	Case 8
k_{xx}	154	0.154	6.54	0.154	77.4	0.462	77.08	100.85
k_{xy}	0	0	-15.83	0	0	0.308	76.92	-73.16
k_{yx}	0	0	-14.31	0	0	0.308	76.92	-73.16
k_{yy}	0.154	154	41.42	30.8	0.154	0.462	77.08	53.31

(b)	*ILSGR*1	*ILSGR*2	*ILSGR*3	*ILSGR*4
m	1	2	3	3
r	5	9	15	15
ϵ_{np}	0	use Eq. (17)	use Eq. (17)	0

Table 1: (a) The values used in the tensor K (b) Acronyms and their meanings in terms of the parameters used for different flux approximation techniques

	(a)			(b)			(c)		
	RMSE	M.E.	T.I.	RMSE	M.E.	T.I.	RMSE	M.E.	T.I.
Case 1	$k_{xx} : k_{yy}$	=	1000:1						
*ILSGR*1	0.138	16.19	22821	0.156	19.13	16350	0.151	17.65	40863
*ILSGR*2	0.012	1.60	23731	0.010	1.30	16448	0.027	3.34	45733
*ILSGR*3	0.012	1.72	23879	0.010	1.36	16396	0.020	2.56	43383
*ILSGR*4	0.106	12.83	23664	0.073	8.56	16293	$*$	$*$	43210
Hybrid	0.066	8.19	28095	0.081	9.62	18829	0.125	14.68	53065
Case 2	$k_{xx} : k_{yy}$	=	1:1000						
*ILSGR*1	0.036	5.707	24112	0.050	8.46	17297	0.069	9.04	31443
*ILSGR*2	0.064	8.30	24234	0.058	7.69	17583	0.062	7.92	31338
*ILSGR*3	0.007	1.22	24322	0.007	1.46	17602	0.007	1.26	31906
*ILSGR*4	0.033	5.71	24576	0.52	9.90	17647	0.139	17.21	31813
Hybrid	0.028	3.73	28492	0.037	6.91	21043	0.024	4.33	48616
Case 4	$k_{xx} : k_{yy}$	=	1:200						
*ILSGR*1	0.024	3.52	11680	0.033	4.62	9042	0.042	5.35	21694
*ILSGR*2	0.037	4.65	11746	0.050	6.46	9008	0.030	4.00	21890
*ILSGR*3	0.005	0.75	11755	0.005	0.63	9062	0.005	0.86	21910
*ILSGR*4	0.015	1.68	11783	0.026	3.97	9019	0.016	2.25	21646
Hybrid	0.018	2.51	13973	0.027	3.87	10472	0.011	2.21	30229
Case 5	$k_{xx} : k_{yy}$	=	500:1						
*ILSGR*1	0.126	14.96	17474	0.145	17.66	12536	0.148	17.52	35261
*ILSGR*2	0.008	1.10	17756	0.008	1.03	12678	0.017	1.84	37708
*ILSGR*3	0.009	1.26	17911	0.008	1.11	12531	0.014	1.99	34716
*ILSGR*4	0.075	9.62	17790	0.047	6.00	12784	$*$	$*$	36607
Hybrid	0.046	5.58	19946	0.056	7.08	13935	0.105	12.82	39195

Table 2: Summary of results on (a) the coarse mesh, (b) the very coarse mesh and (c) the distorted mesh. RMSE - root mean square error. M.E.- maximum error. T.I - total number of *BiCGSTAB* iterations. $*$ - Numerical scheme diverged.

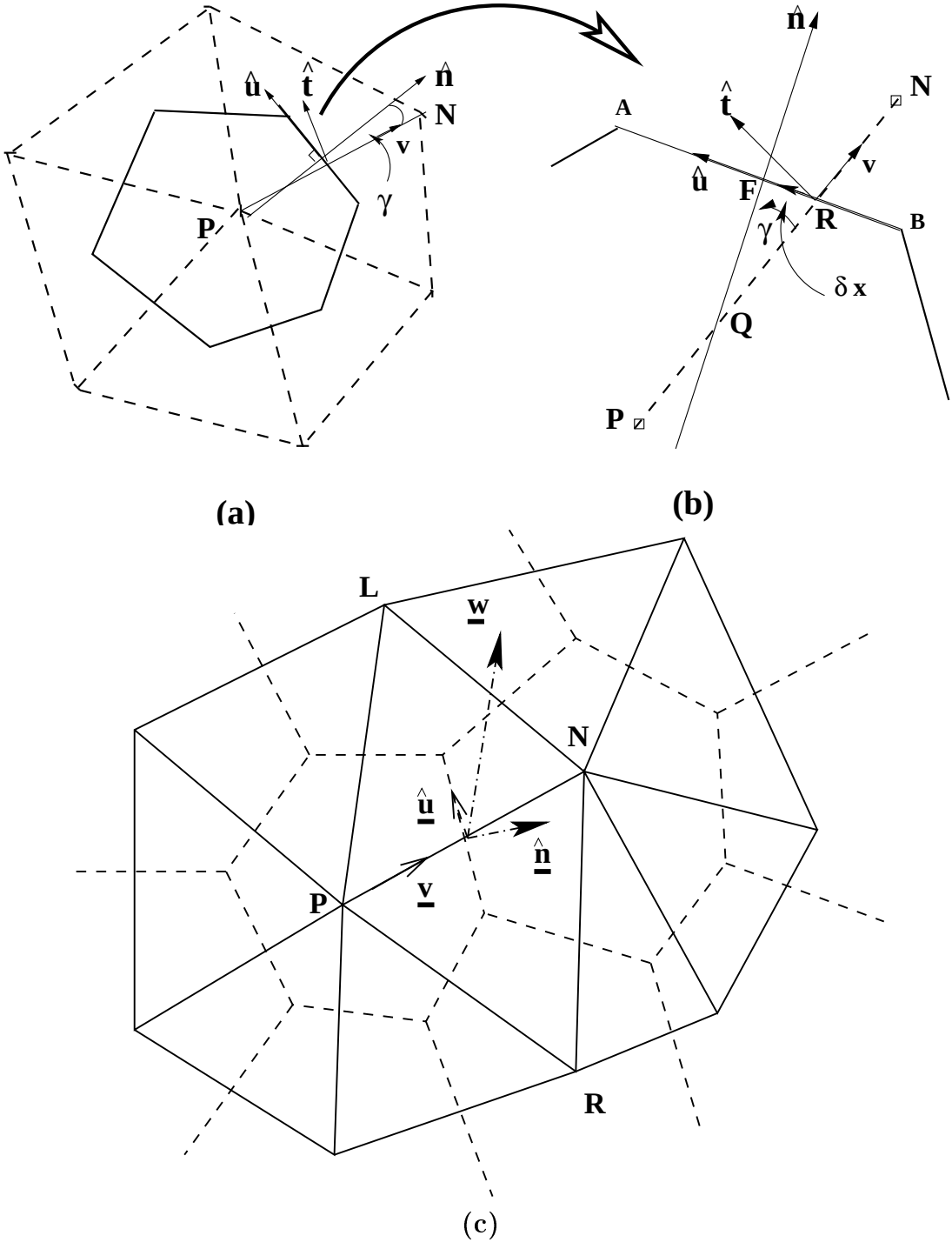

Figure 1: Control volume schematics used for the development of the proposed flux approximation.

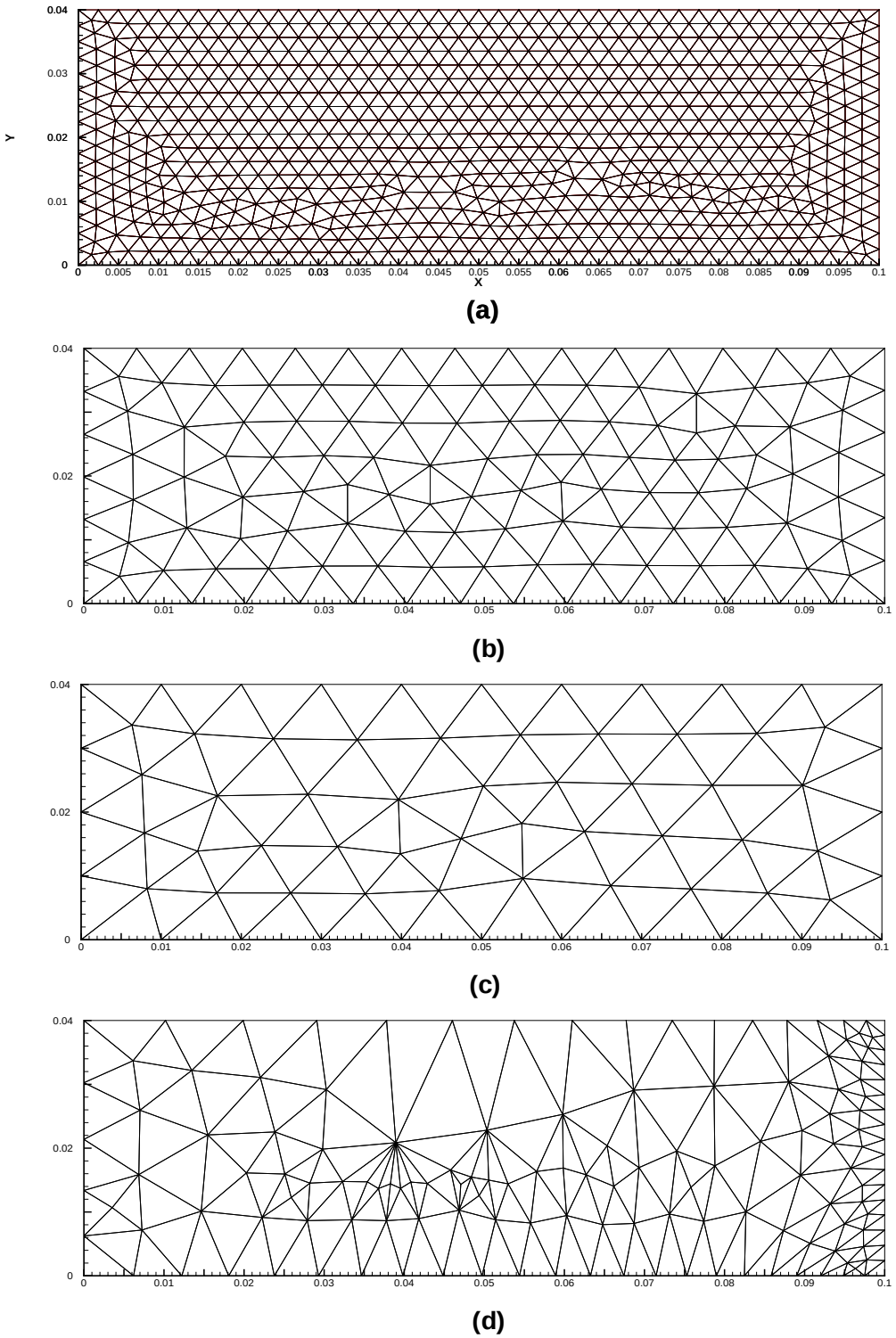

Figure 2: (a) A fine mesh (809 nodes, 1504 elements), (b) a coarse mesh (131 nodes, 218 elements), (c) a very coarse mesh (68 nodes, 106 elements), and (d) a distorted mesh (150 nodes, 237 elements).

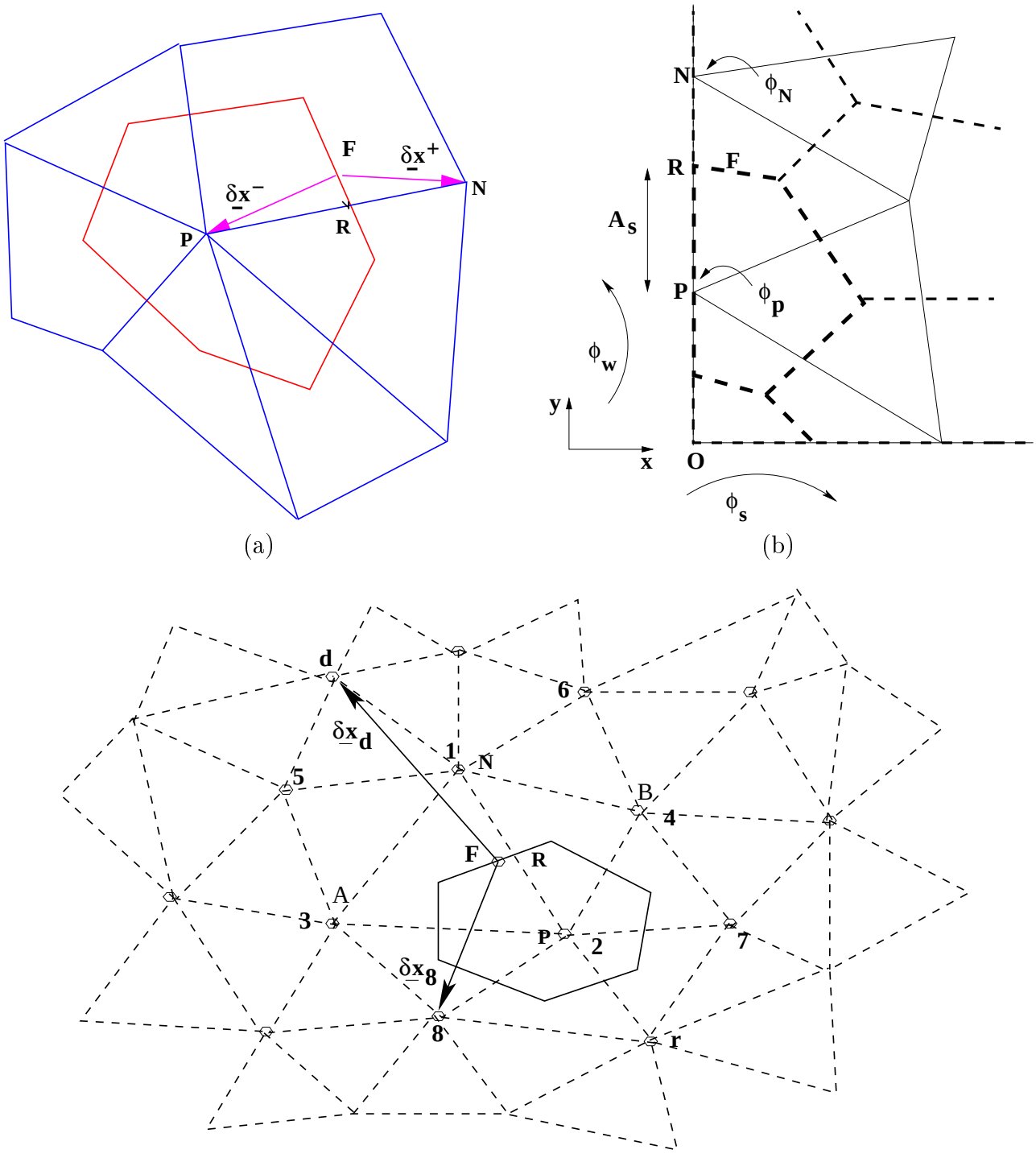

Figure 3: (a) Representative vectors used in Taylor series for determining the correction ϵ_{np}. (b) A typical boundary control volume. (c) A possible distribution of nodes considered for the flux approximation on a CV face.

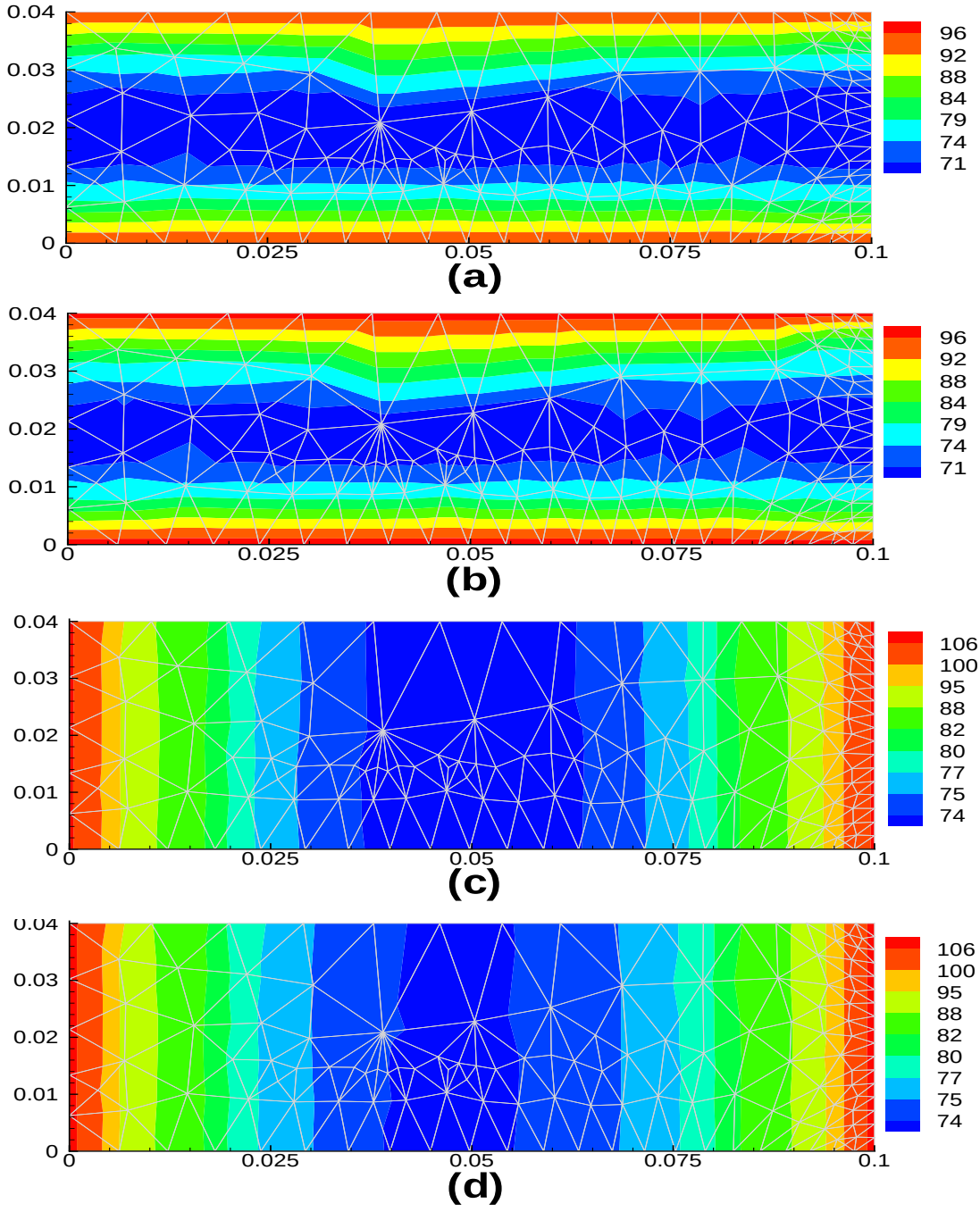

Figure 4: Results on the distorted mesh (Figure 2d) for cases 1 and 2. (a) $k_{xx} : k_{yy} = 1000 : 1$ - exact. (b) $k_{xx} : k_{yy} = 1000 : 1$ - *ILSGR*3. (c) $k_{xx} : k_{yy} = 1 : 1000$ - exact. (d) $k_{xx} : k_{yy} = 1 : 1000$ - *ILSGR*3.

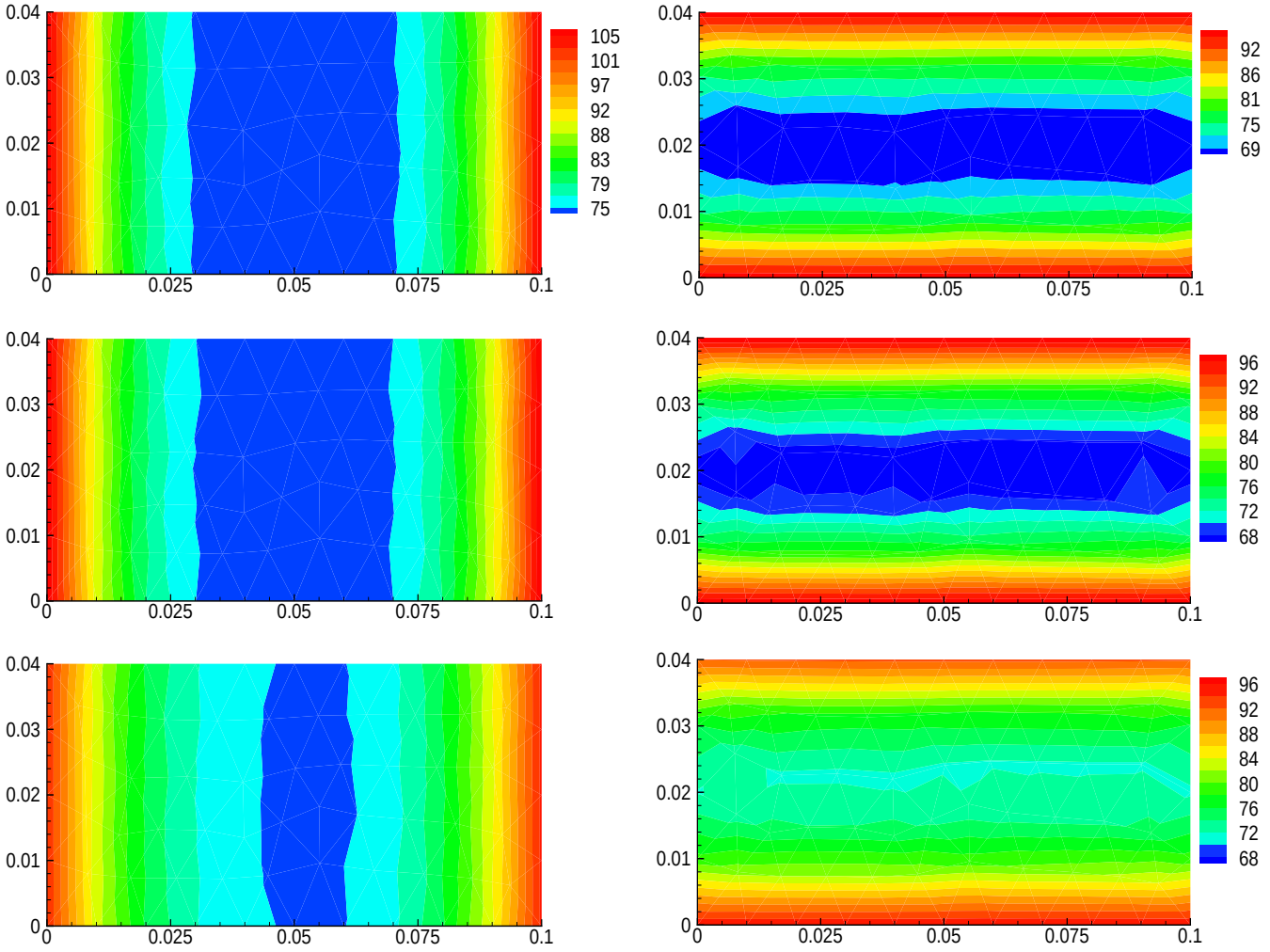

Figure 5: Results for the cases (a) $k_{xx} : k_{yy} = 1 : 200$ and (b) $k_{xx} : k_{yy} = 500 : 1$ on the very coarse mesh (Figure 2c) for cases 4 and 5. Top: Exact, Middle: $ILSGR3$, Bottom: $ILSGR4$

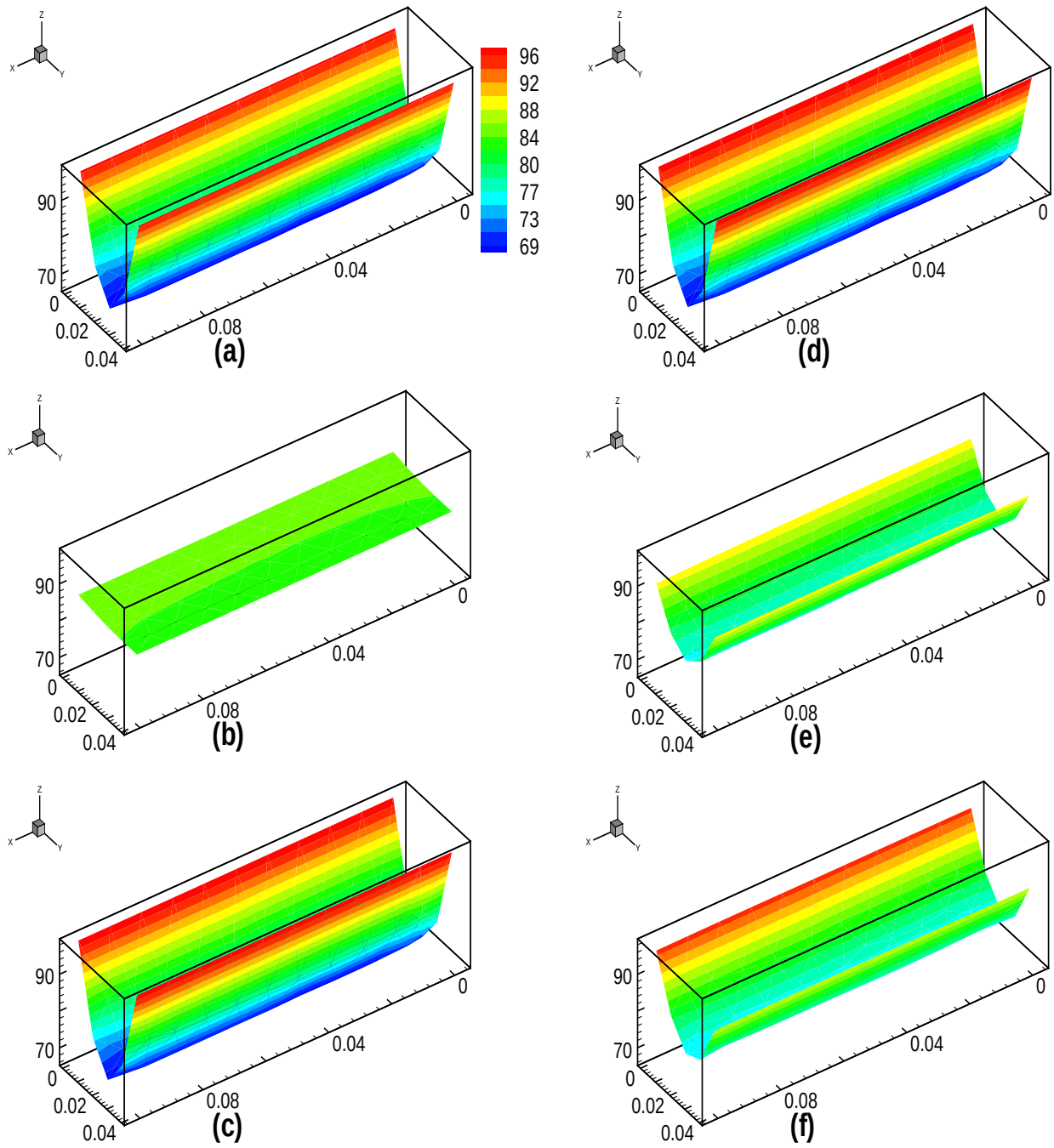

Figure 6: Comparison of results on the very coarse mesh (Figure 2c) for the case 1; k_{xx} : $k_{yy} = 1000 : 1$ (a) exact, (b) $ILSGR1$, (c) $ILSGR2$, (d) $ILSGR3$, (e) $ILSGR4$, (f) Hybrid

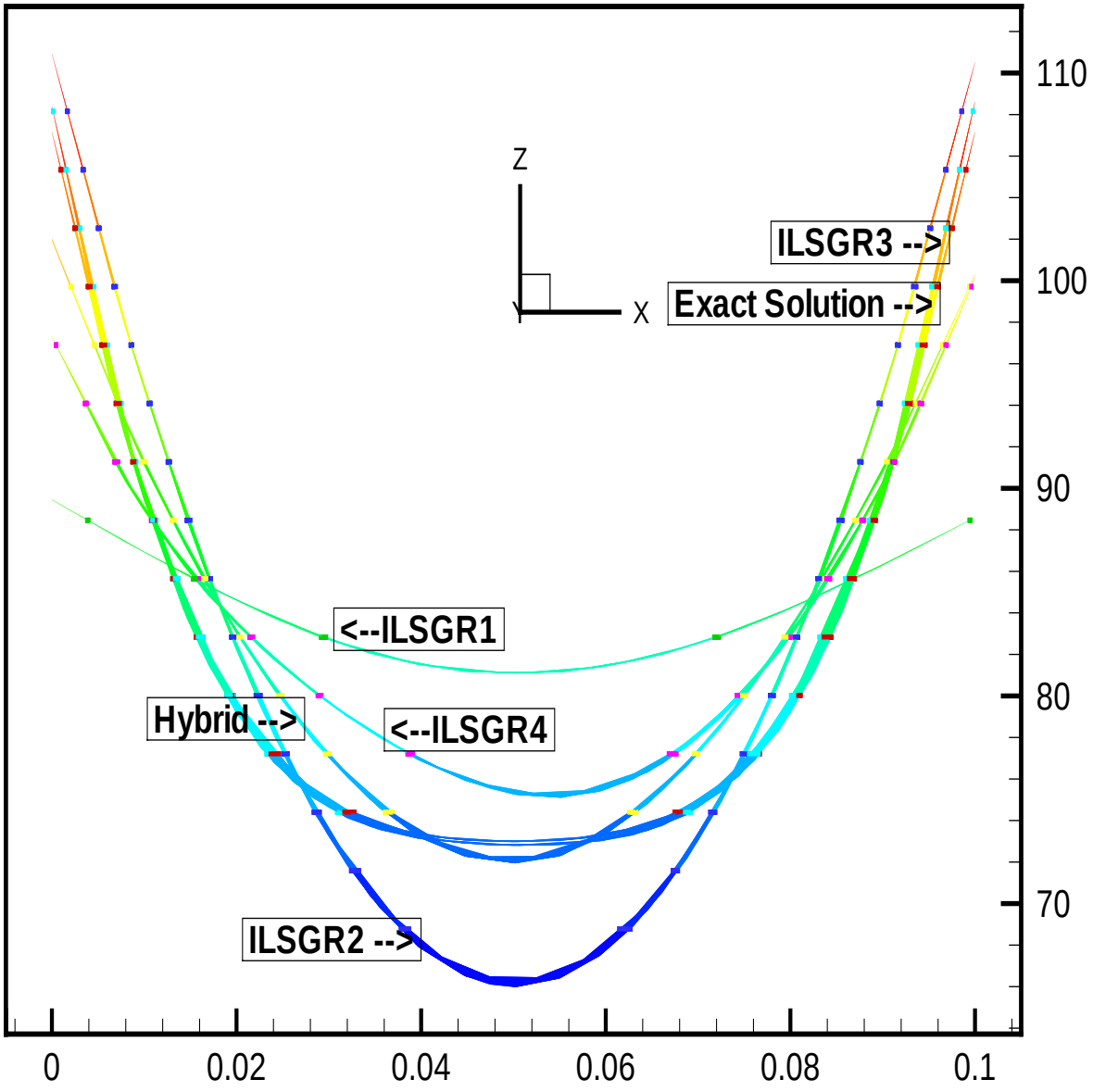

Figure 7: Results on the very coarse mesh (Figure 2c) for the case 2; $k_{xx} : k_{yy} = 1 : 1000$

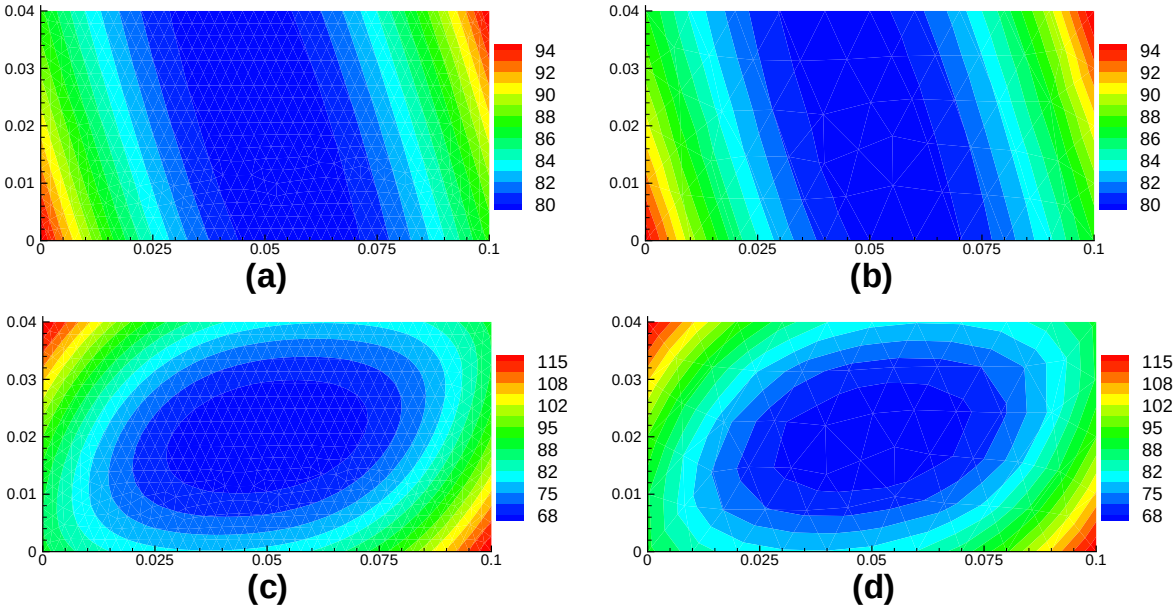

Figure 8: Results using *ILSGR*3: (a) and (b) for case 3. (c) and (d) for case 6. Left column: on the very fine mesh. Right column: on the very coarse mesh.

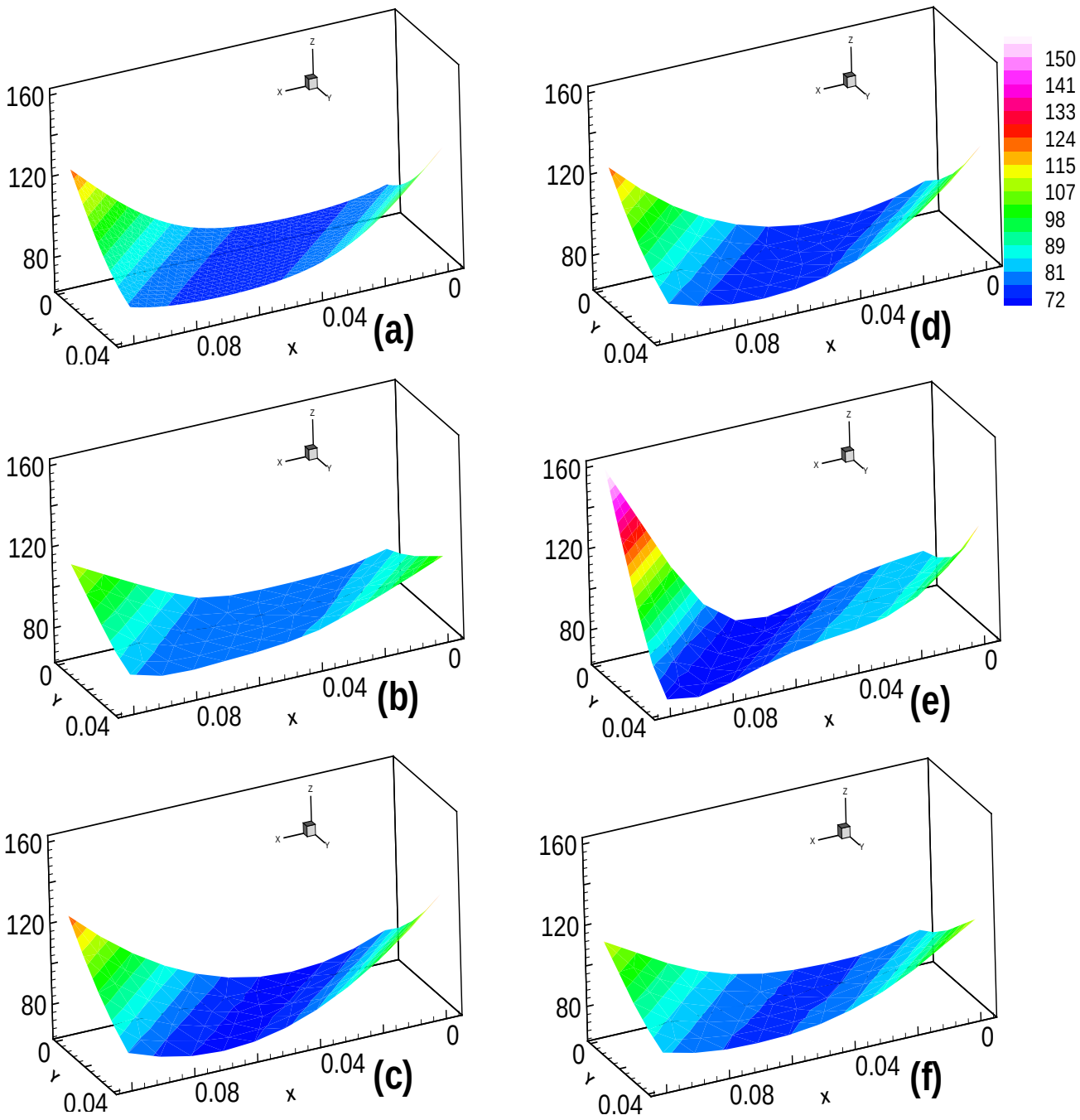

Figure 9: Results for case 7 (a) *ILSGR*3 on the fine mesh. (b) *ILSGR*1 (c) *ILSGR*2 (d) *ILSGR*3 (e) *ILSGR*4 (f) Hybrid on the very coarse mesh.

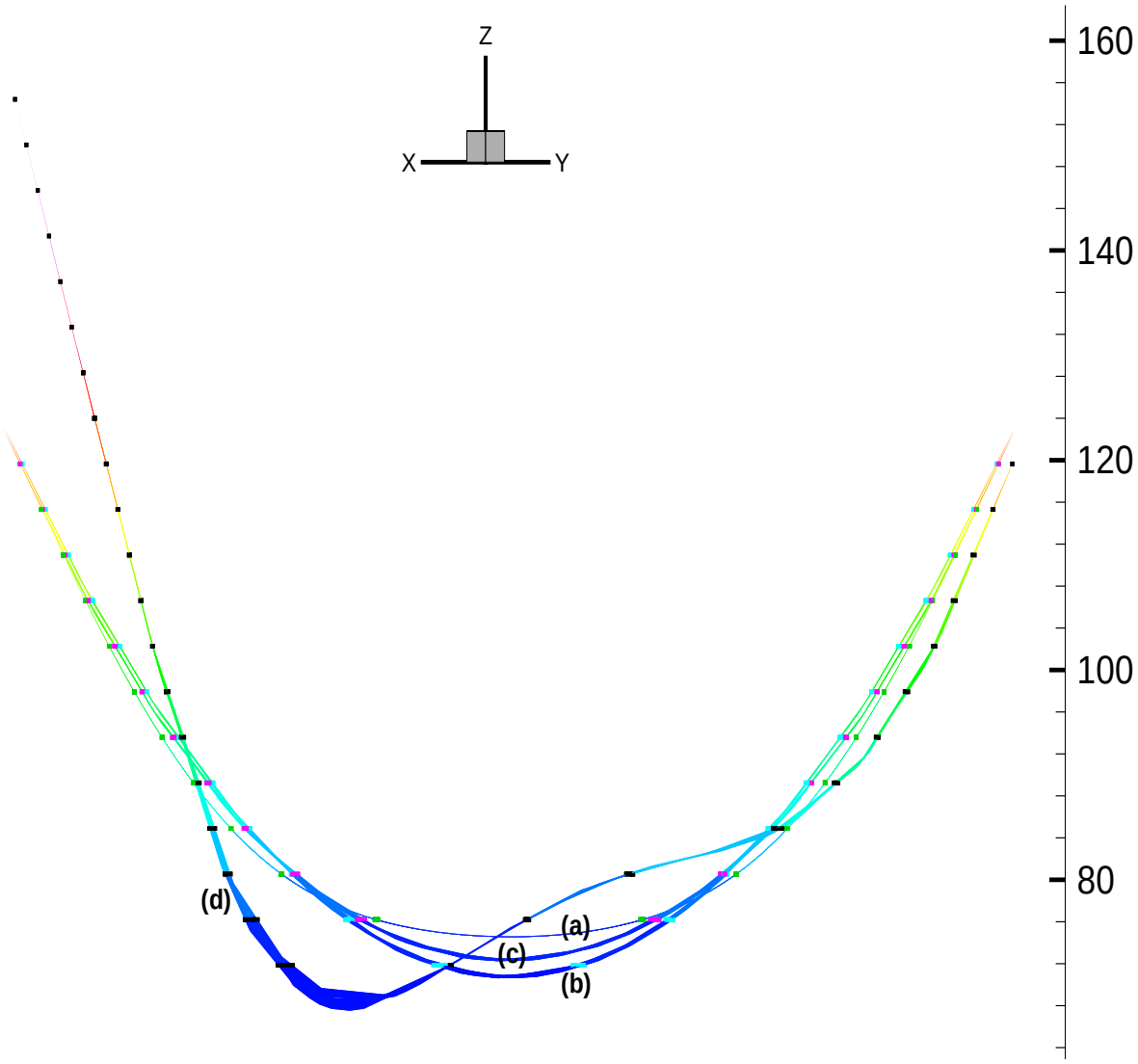

Figure 10: Results for case 7 (a) *ILSGR*3 on the fine mesh. (b) *ILSGR*2 (c) *ILSGR*3 and (d) *ILSGR*4 on the very coarse mesh.

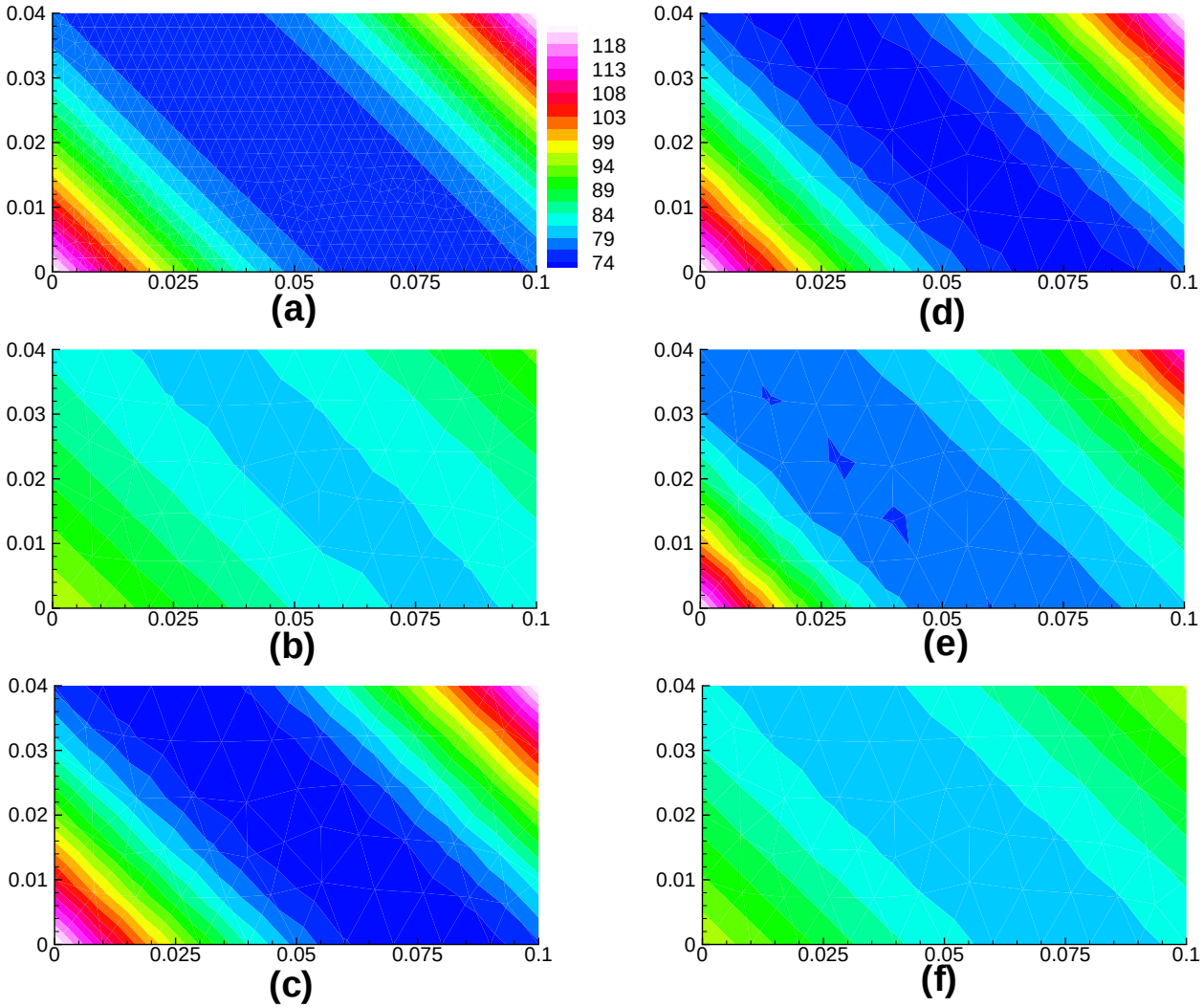

Figure 11: Results for case 8 (a) *ILSGR*3 on the fine mesh. (b) *ILSGR*1 (c) *ILSGR*2 (d) *ILSGR*3 (e) *ILSGR*4 and (f) Hybrid on the very coarse mesh.